USGS Award Numbers: G16AP00102 (PHW, THD), G16AP00103 (LAO)

Title of award: Collaborative Research with University of South Florida and University of Cincinnati: Terrestrial Cosmogenic Nuclide Dating for Determining Slip Rates along Calico Fault, Eastern California Shear Zone

Authors:
Paul H. Wetmore
NES 107
School of Geosciences
University of South Florida
Tampa, FL 33620
P: 813-9744655, F: none, email: wetmore@usf.edu

Lewis A. Owen
Department of Geology
University of Cincinnati
PO Box 210013
Cincinnati, OH 45221-0013
P: 513-5564203, F: 513-5566931, email; Lewis.Owen@uc.edu

Timothy H. Dixon
NES 107
School of Geosciences
University of South Florida
Tampa, FL 33620
P: 813-9740152, F: none, email: thd@usf.edu

Term covered by the award: March 30, 2016 – March 30, 2017

Abstract: Fault slip rate is fundamental to accurate seismic hazard assessment. In the Mojave Desert section of the Eastern California Shear Zone previous studies have suggested a discrepancy between short-term geodetic and long-term geologic slip rate estimates. Understanding the origin of this discrepancy could lead to better understanding of stress evolution, and improve earthquake hazard estimates in general. We measured offsets in alluvial fans along the Calico fault near Newberry Springs, California, and used exposure age dating based on the cosmogenic nuclide ^{10}Be to date the offset landforms. We derive a mean slip rate of 3.6 mm/yr, representing an average over the last few hundred thousand years, significantly faster than previous estimates.

This Final Report is the draft of a manuscript that will be submitted for publication in an open literature, peer-reviewed journal.

Report:

1. Introduction

The Eastern California Shear Zone (ECSZ) accommodates ~20–25% of Pacific-North America plate motion in central and southern California northeast of the "Big Bend" of the San Andreas fault [Dokka and Travis, 1990a,b; Sauber et al., 1994; Dixon et al., 1995, 2000; Miller et al., 2001]. Most of the remaining plate motion is accommodated to the west, on the San Andreas fault in central California, or the San Andreas, San Jacinto and Elsinore faults in southern California [e.g., Bennett et al., 1996; Meade and Hager, 2005; Shen et al., 2011]. ECSZ formation is kinematically linked to the big bend, whose formation in turn is related to the inland jump of the southern part of plate boundary at ~12–5 Ma [Atwater and Stock, 1998; McQuarrie and Wernicke, 2005]. Several faults within the ECSZ likely formed or accelerated around this time [Dokka and Travis, 1990a,b]. The region has been an important "natural lab" to study the formation and evolution of faults [Frankel et al., 2008], as well as other tectonic and plate kinematic studies, including the classic study of Minster and Jordan [1987]. These authors first identified the "San Andreas discrepancy" as a key issue; the discrepancy represents the difference between overall plate motion, and motion carried by the San Andreas fault. This discrepancy was initially attributed to significant right-lateral shear on other faults, within the Basin and Range province to the east, and the California continental margin to the west [Minster and Jordan, 1987; Ward, 1990].

More recently, several authors [e.g., Gan et al., 2000; Meade and Hager, 2005; Spinler et al., 2010; Evans et al., 2016] have noted discrepancies between geologically determined versus geodetically determined slip rate estimates for individual faults within the ECSZ, or for summed rates across shear zone, hereafter termed the ECSZ discrepancy. For example, in the Mojave Desert region (Figure 1), summed geologic slip rate across the region at ~34.8°N is ≤6.2±1.9 mm/yr [Oskin et al., 2008], while geodetic rate estimates are significantly faster, ~11 mm/yr to ~18 mm/yr [Evans et al., 2016 and references therein] (Figure 2). For individual faults, published studies suggest that the Calico fault has the fastest geological slip rate (at 1.8±0.3 mm/yr) [Oskin et al., 2007, 2008], and the fastest geodetically-derived slip rate (e.g., 11.7±2.6 mm/yr by McGill et al. [2015]). These discrepancies have been attributed to a variety of causes, including:

1. Off-fault deformation, such that fault rates sensu stricto are less than the integrated block motion rate, e.g., Shelef and Oskin [2010], Dolan and Haravitch [2014], and Herbert et al. [2014a].

2. On-going acceleration of ECSZ faults, such that the geologic rate estimate (by definition, a long-term average) averaged over the early stages of the fault's activity will be less than the geodetic rate [Gourmelen et al., 2011].

3. The effects of post-seismic motion and visco-elastic relaxation, such that geodetic rates within a few years or decades of a major earthquake are faster than their long term average [Dixon et al., 2003; Chuang and Johnson, 2011; McGill et al., 2015]. In other words, the rates differ only because the long-term rate is not modeled properly in most geodetic approaches, which assume elastic rheology.

4. There are true long term differences in the fault slip rates, reflecting fundamental processes in the tectonic and seismic evolution of the ECSZ region, such as transient strain on individual faults, or temporally clustered earthquakes at the scale of the shear zone [Rockwell et al., 2000; Peltzer et al., 2001; Meade and Hager, 2005; Dolan et al., 2007; Oskin and Iriondo, 2004; Oskin et al., 2007, 2008; Cooke and Dair, 2011].

Determining the origin of such discrepancies, in the ECSZ and elsewhere, is important for a variety of reasons, including improved understanding of earthquake processes and fault evolution, as well as seismic hazard assessment. In its simplest form, seismic hazard for a given fault is linearly related to the fault's slip rate: such that faster faults are likely to have more frequent earthquakes than slower faults.

One explanation that has not been adequately explored is the fact that geologically determined slip rates are by definition minimum rates. This reflects the fact that the offset used to define the rate may start a considerable amount of time after the feature formed [Dawson and Weldon II, 2013]. Only by sampling a large number of offset features of various ages is it possible to gain confidence in the geologically determined slip rate estimate. Assuming that there are no systematic errors in the rate estimate, the best estimate of rate is not the average of the ensemble of rate estimates, but the fastest one. To our knowledge, no fault in the Mojave ECSZ region has been studies sufficiently to generate the necessary ensemble of rate estimates.

Here, we review geodetic and geologic slip rate estimates for the region, and report a new geological slip rate estimate for the Calico fault, a major fault within the Mojave Desert section of the ECSZ. The new rate is significantly faster than previously determined rates, and hence bears on the issue (and perhaps the reality) of the ECSZ discrepancy.

2. Previous work

2.1. Prior geodetic studies

Fault slip rate estimates from geodetic data are model-dependent. Most models assume either a purely elastic rheology or an elastic layer overlain on one or more visco-elastic layers. The latter has been used to study earthquake-cycle effects in the ECSZ [Malservisi et al., 2001; Dixon et al., 2003; Chuang and Johnson, 2011]. However, Meade and Hager [2005] used an elastic model to test the time-dependent deformation and found no significant long-term post-seismic relaxation in southern California, concluding that the viscosity of the lower crust/upper mantle is relatively high.

Elastic block models suggest ~11 to ~18 mm/yr of cumulative slip rate across the region [Evans et al., 2016 and references therein] (Figure 2). Some authors point out that the largest discrepancy is concentrated on the Calico fault, located between the ruptures of the 1992 M_w 7.3 Landers and 1999 M_w 7.1 Hector Mine earthquakes [McGill et al., 2015; Evans et al., 2016]. They suggest that the discrepancy between geodetic and geologic slip rates in the ECSZ is related to these two large earthquakes, which causes visco-elastic deformation in the mantle that varies over the time scale of an earthquake cycle. Liu et al. [2015] used historical triangulation/trilateration observations before the Landers earthquake and GPS measurements after the Landers earthquake to recover the secular deformation field and differentiate the post-seismic transients. They found that the Landers and Hector Mine earthquakes adversely affect GPS measurements, with 2–3 mm/yr excess right-lateral shear across the co-seismic ruptures in the GPS solutions. They estimated a cumulative deformation rate of 13.2–14.4 mm/yr across the Mojave section of the ECSZ, similar to the pre-Landers geodetic estimate of 12 mm/yr by Sauber et al. [1994].

A highly disconnected fault network in the Mojave ECSZ could imply significant off-fault deformation [Herbert et al., 2014a, b; Selander, 2015]. By studying the deflection of continuous planar markers and the rotation of paleomagnetic sites, Shelef and Oskin [2010] found that distributed deformation can accommodate 0 to ~25% of the total displacement, with deformation focused in zones 1–2 km from the faults.

Herbert et al. [2014b] used a boundary element method to simulate three-dimensional deformation of the ECSZ. This modeling approach suggests that a block-like fault network (faults are simplified to be connected) produces a cumulative strike-slip rate 36% greater than a discontinuous fault model. Based on gradients in the derived deformation map and the implied strain energy density, Herbert et al. [2014a] concluded that 40±23% of the total strain across the ECSZ could be attributed to off-fault deformation.

Evans et al. [2016] used a total variation regularization method to investigate the role of fault system geometry in block models, determining a best-fitting geometry from an initial model with numerous faults. This method could minimize the influence of fault geometry assumptions and reduce uncertainties in geodetic slip rate estimates. Moreover, since a dense fault geometry was used in the initial model, which included active faults separated by <10 km, this modeling method should be able to assess the role of distributed deformation. Evans et al. [2016] identified persistent discrepancies between geologically and geodetically estimated slip rates in the ECSZ, with 4–7 mm/yr discrepancies on the Calico fault. This suggests that inconsistencies between geology and geodesy cannot be due exclusively to off-fault deformation.

2.2. Prior geological studies

Assuming a fault initiation time of ~10.6–5.5 Ma and a total of 65 km right slip displacement at 35° N, Dokka and Travis [1990a, b] estimated the integrated long-term slip rate of the ECSZ at 6–12 mm/yr.

Oskin et al. [2008] measured the surface displacement of alluvial fans and a lava flow, determining the slip rates of six dextral faults across the ECSZ, with an overall rate of ≤6.2±1.9 mm/yr at ~34.8°N. In this study, the Calico fault had the fastest slip rate, at 1.8±0.3 mm/yr. Oskin and Iriondo [2004] estimated 0.5 mm/yr slip rate of the Blackwater fault to the north of the Calico-Blackwater fault system. Selander [2015] interpreted such rate fluctuations as evidence for strain transfer from the Calico fault across the Manix Basin onto the Harper Lake faults, Mud Hills thrust, and Tin Can Alley fault, with overall dextral slip apparently decreasing to the northwest to ≤2.6±1.9 mm/yr north of 35°N.

3. New displacement observations

Our study area is located near Newberry Springs, California (Figure 1). Two alluvial fan surfaces here are offset by the Calico fault (Figure 3). We refer to them as the Autumn Leaf Road (ALR) and Troy Road (TR) alluvial fans based on nearby roads. Three techniques were used to study the alluvial fans and estimate their strike-slip displacements: (1) Field mapping, (2) high resolution aerial orthoimagery (USGS EarthExplorer) with ~0.3 m horizontal resolution, and (3) Digital Elevation Model (DEM) derived from airborne LiDAR data (OpenTopography Facility) with 0.5 horizontal resolution and centimeter-level vertical precision. Techniques (2) and (3) are especially useful in this semi-arid environment.

3.1. Autumn Leaf Road alluvial fan

The ALR alluvial fan is the oldest observed alluvial fan surface in the Newberry Springs area and is represented by a series of isolated alluvial surfaces elevated 2-3 m above younger surfaces cut into the older deposit (Figure 3). The alluvial fan surface is defined by a well-developed desert pavement, dominated by dark varnished pebbles and abundant, but spaced, surrounded to sub angular boulders with compositions that include quartzite, basalt, granite and rhyolites (Supplementary Figure S1). Fault traces identified by field mapping and aerial photography show a well-defined linear trend striking northwest 323°-143°. The Calico fault cuts the alluvial fan, with the main body to the southeast and three smaller alluvial fan surfaces to the northwest. The alluvial fan surface is also characterized by shallow channels that are partially filled, with one prominent (1-2 m deep) drainage on both the southeast alluvial fan portion and the most northwesterly of the three smaller surfaces (marked by yellow dots on Figure 4). Excavation of a 2 m deep trench within the ALR alluvial fan reveals that the deposit is dominated by cobbles with rare boulders, and the development of calcium carbonate coatings of a few millimeters thickness with some weak conjoining of adjacent clasts.

We reconstructed the pre-displacement ALR alluvial fan along the fault trace based on soil development and the LiDAR DEM, obtaining 1120±55 m of right-lateral displacement (Figure 4). This places the largest of the three smaller alluvial fan surfaces immediately adjacent to the southwestern margin of the main body northeast of the Calico fault. This also aligns the major channel (between the cyan and green dots in Figure 4a) on both sides of the fault, and the main drainage on the alluvial fan surfaces (marked by yellow dots in Figure 4a). The half width of the major channel (55 m) has been used to estimate the 1σ error for this displacement. For consistency with previous studies (e.g., Oskin et al., 2007, 2008; Selander, 2015), we quote 2σ error space (95% confidence interval) as the uncertainty in following discussion.

3.2. Troy Road alluvial fan

The TR alluvial fan is located ~1 km southeast of the main body of the ALR Fan (Figure 3). Surface varnish development on the alluvial fan surface suggests an intermediate age between the active channel and the ALR alluvial fan surface. A network of partly filled channels and trains of 0.5–1 m scale boulders characterize the alluvial fan surface. Well-preserved bars with imbricated boulders are pervasive across the alluvial fan surface. Carbonate coatings and rubification of the undersides of clasts and boulders are uncommon to non-existent within this fan. The TR alluvial fan has been eroded away along both its northwestern and southeastern margins, with many active channels from southwest to northeast (Figures 3 and 5). Our mapped fault traces show that the Calico fault transfers slip from south-north to southeast-northwest trend as it passes this alluvial fan, and produces some secondary fault traces near the main fault scarp. At the offset of this alluvial fan, the fault strikes 338° (Figure 3).

Northwest of the TR alluvial fan, there is an inter-mediate surface that increases the uncertainty of the displacement estimate. When aligning the linear active channel downstream with the northwestern edge of the oldest TR alluvial fan surface, the estimated displacement is 90 m (Figure 5 a2, b2, c2). However, using the slope aspect map derived from the LiDAR DEM (Figure 5 c1) suggest that the intermediate surface adjacent to the oldest alluvial fan surface has a slope trending towards the northwest, which is the same as the main TR alluvial fan surface. If we align the northwestern most edge of the inter-mediate surface with the downstream channel, the displacement estimate is 205 m (Figure 5, a3, b3, c3). We therefore take 90 m as the minimum estimate and 205 m as the maximum estimate for the displacement on TR alluvial fan.

4. Terrestrial cosmogenic nuclide ^{10}**Be** exposure dating

Rock samples were collected from surface boulders and cobbles on the ALR and TR alluvial fan surfaces, and sediment deposits were collected from two depth profiles: CalicoA for the ALR alluvial fan and Calico-Pit2 for the TR alluvial fan (Figure 3b). These samples are used for terrestrial cosmogenic nuclide (TCN) ^{10}Be age dating. Rock samples were picked based on similar criterion as described in Gray et al. [2014], Frankel et al. [2015] and Hedrick et al. [2016]: 1) Large, typically >50 cm in length; 2) Stable, boulders inset into the ground were preferred; 3) Little sign of erosion; and, 4) Quartz rich lithology. For places where boulders were absent, whole cobbles were collected. Trench sites were chosen to be located at the highest areas on their respective alluvial fan surfaces and seemed to have experienced little surface erosion. All rock samples have been prepared by standard processing procedures, including rock crushing, magnetic separation, mineral separation (for some samples), etching, dissolution, purification, and target loading. Depth profiles have gone through the same processing procedures except for rock crushing: we sieved sand grain sizes between 0.25 mm and 0.5 mm for the procedures afterwards as described above. However, sand samples from trench Calico-Pit2 did not yield sufficient volumes, thus small pebbles, with size between 0.5 mm and 12.5 mm were crushed to increase the amount of quartz for processing. Detailed descriptions of these samples and the TCN sample processing steps are given in the Supplementary materials. Uncertainties for all ages are estimated at 2□ (95% confidence interval).

4.1. Autumn Leaf Road alluvial fan

Ten rock samples on the ALR alluvial fan surface yield ages that range from 75.3 to 345.7 ka (Figure 6a, Supplementary Table S1 and Figure S3). Eight have ages of ~100 ka, while the other two have ages that are >300 ka. Sample ages of ~100 ka would give a slip rate that is unrealistically high (>10 mm/yr), . Therefore we interpret them as disturbed (Figure 6). A Monte Carlo simulation method [Zechar and Frankel, 2009] for the other two rock samples with age >300 ka gives the age estimate to be 328.4 $^{+37.9}/_{-32.0}$ ka. To incorporate different age estimates and be easily applied to slip rate estimates when displacement errors are given in normal distribution, errors from Monte Carlo simulation approach were simplified as symmetric distribution and the wider error sides were used as uncertainties for further incorporation. This does not change interpretations to the results because the difference between two sides in asymmetric error distribution are small compare to the corresponding age estimates (<2% for rock samples and <10% for depth profile of ALR alluvial fan, <15% for rock samples of TR alluvial fan).

To better constrain the results, samples collected at various depths from a trench at the southern corner of the main body of ALR alluvial fan were used to help assess the exposure ages. we expected an exponential decrease in concentration versus depth if the fan body formed in an alluvial way. Figure 7 shows the concentration versus depth and age estimate based on the depth profile CalicoA, and ^{10}Be concentrations show a decreasing trend with depth. By using a Bayesian-Monte Carlo simulation method [Hidy et al., 2010; Hidy, 2013], we estimate the surface age at this location to be 204.5 $^{+91.7}/_{-71.9}$ ka and the inheritance age is ~7.6 ka. The upper bound of surface exposure age agrees with age estimate from rock samples within 2□ if they have the same inheritance as estimated from the depth profile. However, the relative small inheritance estimated from CalicoA and the complex nature of inheritance prevent us from subtracting inheritance age in the rock samples, therefore we use apparent ages for rock samples, this won't change the interpretation to our age estimates. Combine the age estimate from the depth profile (204.5±91.7 ka) and the Monte Carlo estimate (328.4±37.9 ka) from surface rock samples, the weighted mean age and uncertainty is 310.3±35.0 ka. We use this as the exposure age for the ALR alluvial fan, which is probably the maximum age as it may contains a low inheritance age (7.6 ka from CalicoA).

4.2. Troy Road alluvial fan

Among nine dated rock samples collected on the TR alluvial fan surface, one (Calico-6) has an age of 249.7 ka. This is incompatible with the observed soil development here. Large inheritance from other older units likely explains this anomalously old age, and this age is not included in the subsequent discussion. The remaining eight samples have ages that range from 10.9 ka to 69.9 ka, but fall into two sets: four of the eight samples cluster between 10.9 ka and 17.1 ka, while the other four cluster between 41.4 ka and 69.9 ka (Figure 8 and Supplementary Figure S3).

The depth profile Calico-Pit2 was not useful for constraining the age estimate because there was no significant exponential decrease in ^{10}Be concentrations with depth as is necessary to estimate the surface exposure age based on a concentration versus depth profile (Figure 9). We interpret this to indicate inheritance saturation, and may be partly explained by the amalgamation of sand and pebbles for samples from Calico-Pit2, which could disturb the ability to model ages with depth profiles [Hidy et al., 2010].

For the two age clusters from rock samples, if the younger suite of ages represent the true exposure age, this suggests an inheritance+exposure age for the TR alluvial fan to be less than 17.1 ka, which is incompatible with the inheritance saturation (equals to ~57 ka) from depth profile Calico-Pit2. On the other hand, if the saturated depth profile suggests a young age (i.e., 10.9–17.1 ka), the inheritance age would be >30 ka, much higher than the apparent ages of the younger cluster, which is unlikely to be true because surface sample ages contain a combination of inherited and exposed concentrations of ^{10}Be. For comparison, Oskin et al. [2007] used samples collected on the wash beside their "K" surface (age: 56.4 ka, ~6 km to the southeast of our sampling site) to estimate the ^{10}Be inheritance, and they estimated a very low inheritance value (1.7 ka). We also notice that rock samples in the younger age cluster were located relatively close to the fault scarp (<50 m, Figure 3 and Supplementary Figure S3), and there is at least one distinct secondary fault trace nearby (Figure 3), which may imply a complex transport history for these rocks. We therefore interpret these samples as disturbed, and use the sample ages between 41.4 and 69.9 ka for age estimate. This argues for an age of 52.9 $^{+23.6}/_{-15.7}$ ka for the TR alluvial fan. If the sample ages of 10.9 ka to 17.1 ka represent the true exposure age of the TR alluvial fan, the Monte Carlo median age of 13.6 ka would yield a slip rate estimate of 6.6 to 15.1 mm/yr, which seems to us unrealistically fast.

5. Slip rate estimate

For the ALR alluvial fan, the displacement of 1120±110 m and TCN exposure age of 310.3±35.0 ka yield a slip rate of 3.6±0.5 mm/yr. For the TR alluvial fan, the minimum displacement of 90 m and a TCN exposure age of 52.9±23.6 ka yields a slip rate of 1.7±0.8 mm/yr. Using the maximum displacement for the TR alluvial fan (205 m) and the same age yields a slip rate of 3.9±1.7 mm/yr (Figure 10).

While both this study and Oskin et al. [2007] show large range of age estimates on single alluvial fan surfaces, we estimate the Calico fault slip rate in our study area as a weighted mean value based on slip rate estimates from the ALR (3.6±0.5 mm/yr) and TR (1.7±0.8 to 3.9±1.7 mm/yr) alluvial fans to avoid over extrapolation of age dating results. The weighted mean slip rate for the Calico fault is between 3.1±0.4 and 3.6±0.5 mm/yr (Figure 10).

6. Discussion

6.1. Spatial or temporal variations in slip rates

Our new slip rate estimate of 3.6±0.5 mm/yr is twice the slip rate estimate of 1.8±0.3 mm/yr from a 56.4±7.7 ka old "K" Fan by Oskin et al. [2007], and more than double the slip rate estimate of 1.4±0.4 mm/yr from a 650 ± 100 ka old "B" Fan by Oskin et al. [2007], and more than double the 1.4 $^{+0.8}/_{-0.4}$ mm/yr estimate from a 17.1 $^{+1.6}/_{-2.6}$ ka old "Q2c" unit southwest of the Rodman Mountains by Selander [2015].

Since these slip rate estimates are based on offsets with different locations and ages, there are three possible explanations for the difference: (1) slip rate on the Calico fault changes along strike; (2) slip rate on the Calico fault changes with time; and, (3) some of the assumptions used to estimate slip rates are in error. Regarding the first explanation, Oskin et al. [2007] and Selander [2015] suggest that slip in the Calico-Blackwater fault system varies spatially, with slip transferring from the Calico fault to the Harper Lake and Blackwater faults via a set of thrust ramps, or absorbed by folding adjacent to the Calico fault. However, our study area is only ~6 km from the study area of Oskin et al. [2007], and ~15 km from the study area of Selander [2015] in the southeast (Figure 11). To support an increase from 1.4/1.8 to 3.6 mm/yr would require the nearby Camp Rock fault (≤1.4 mm/yr) to transfer all its slip to the Calico fault within 15 km. While Selander's [2015] study suggests a systematically decrease pattern of dextral slip rate along the Calico fault northwards from the Rodman Mountains to the Calico Mountains, rapid increase of slip rate from their study sites towards our study area along the Calico fault in such a short distance seems unlikely. As for the second explanation, the age of TR alluvial fan is very close to the age of "K" Fan in Oskin et al. [2007], and slip rate of the "K" Fan falls to the lower end of slip rate estimate from TR alluvial fan. This may imply that the minimum estimate of 90 m is more likely to be the true displacement for the offset of TR alluvial fan. If all these slip rate estimates are correct, this requires that this segment of the Calico fault slips at an increasing rate from ~650 ka to ~310 ka, but then decreases after ~310 ka. While we cannot preclude such a temporal variation, we note that the kinematic boundary condition, Pacific-North America plate motion, has changed less than 2% (<1 mm/yr) since 4.2 Ma [DeMets and Merkouriev, 2016]. If slip switches between different faults within the shear zone fault network in the past ~650 ka, then a ~2 mm/yr slip rate variation on the Calico fault would require corresponding trade-off variations on other faults to balance the stable boundary condition. However, all the other five major dextral faults in the ECSZ have slip rates less than 1.4 mm/yr in the past 37 to 752 ka [Oskin et al., 2008], a complex slip transfer behavior between different faults is needed to fulfill the overall slip rate. Hence it is useful to consider simpler explanations.

Could the different rate estimates be caused by incorrect assumptions used in the slip rate calculations (our 3rd explanation)? For example, offset reconstructions use geomorphic information, but erosion may blur key features. In the case of the TR alluvial fan, the diffuse inter-mediate surface may have been part of an active channel, or part of the TR alluvial fan that was eroded away. This different interpretation changes the slip rate estimate by a factor of 2.3. Since displacement is in the numerator for slip rate estimates, uncertainty in the displacement estimate has more affect on the rate estimate for younger fans. However, older fans may suffer more from erosion. On the other hand, age determinations generally cause even larger uncertainties in slip rate estimates, especially for younger features. In this study, rock samples from both the ALR and the TR alluvial fan have large age ranges, cautions are needed in interpreting these ages. Ideally, more than one technique should be used [Oskin et al., 2007, 2008; Owen et al. 2011]. In this study, however, these alluvial fans are too old for ^{14}C dating, and no appropriate material were collected for OSL or U-series dating, so we only use ^{10}Be TCN ages. While ^{10}Be TCN has been widely used for surface exposure dating, the technique relies on numerous assumptions for both pre- and post-formation history, including inheritance, fault activity, erosion, shielding, etc.. Figure 12 shows the age distribution from samples collected in ALR alluvial fan. Although most rock samples have age estimates ~100 ka, we interpreted them as disturbed. Many reasons can explain such phenomenon, for example: though rock samples we choose have no apparent sign of erosion or toppling, however, in the long period since the formation of the alluvial fans, some factors can prevent rocks from continuously exposed to the cosmic rays, such as strong earthquakes could topple surface boulders or cobbles, wind and flood could roll rocks over, vegetation could shield them against the cosmic rays, etc.. These would lead the rocks samples have younger age estimates than the offset age of the alluvial fan. The large range of age estimates from this study illustrates the challenge of using ^{10}Be TCN to date alluvial fans along the Calico fault in Newberry Spirngs area.

6.2. Cumulative slip rate across the ECSZ

If our new slip rate estimate of 3.1±0.4 to 3.6±0.5 mm/yr is correct, then the cumulative geologic slip rate for all six of the major dextral faults comprising the Mojave ECSZ at ~34.8° N is 7.5±0.9 to 8.0±0.9 mm/yr, using the data from Oskin et al. [2008] for the other five faults (Figure 13 and Supplementary Figure S4). Given the fact that faults in the Mojave Desert section of ECSZ are highly discontinuous and all faults are immature (i.e., total offset for individual fault is ≤25 km [Dolan and Haravitch, 2014], and total offset for faults in the Mojave ECSZ are all ≤21.5 km [Dokka and Travis, 1990a]), the slip rates we derived should miss significant amounts of off-fault deformation [Dolan and Haravitch, 2014]. If off-fault deformation is as high as 40% in this region (as suggested by Herbert et al. [2014a]), then overall geologic displacement rate across the Mojave Desert would be 10.5±0.9 to 11.2±0.9 mm/yr.

For comparison to geodetic estimates, we consider three approaches. First, we have the pre-Landers estimate of 12±2 mm/yr of Sauber et al. [1994] based on terrestrial geodetic data. Second, we can use post-Landers GPS data, corrected for post-seismic effects. Liu et al. [2015] use this approach to estimate a secular rate of 13.2–14.4 mm/yr. Third, we can look at geodetic data north of the Garlock fault, which is much less affected by post-seismic motion from the Landers and Hector Mine earthquakes. The overall rate of plate motion is virtually identical between southern and central California [DeMets and Dixon, 1999; DeMets et al., 2010; DeMets and Merkouriev, 2016], and we are not aware of any structures that would radically change the nature of partitioning. We compared transects north (T1) and south (T2) of the Garlock fault (Figure 14) and estimated the summed geodetic slip rate for northwest-directed dextral shear east of the San Andreas fault, using the MIDAS GPS data set [Blewitt et al., 2016]. Details of the estimation procedure are given in the Supplementary materials. We obtain a rate of 11.2±0.6 mm/yr for both transects, similar to the pre-Landers estimate of total slip rate across the Mojave ECSZ [Sauber et al., 1994], and similar to our new geological estimate.

While there are still considerable uncertainties in these various estimates, it seems reasonable to conclude that available data do not require a discrepancy between geological and geodetic slip rate estimates in the Mojave section of the ECSZ.

6. Conclusion

The faster slip rate estimate (3.1±0.4 to 3.6±0.5 mm/yr) for the Calico fault in this study highlights the possibility that some fault slip rates in the Mojave desert have been underestimated. Presumably this underestimate is caused by limited number of studies and inappropriate assumptions in displacement and age estimates. The overall ~11 mm/yr geodetic slip rate may be balanced by geologic rate if the new estimate in this study represents the slip rate of the Calico fault.

Considering numerous faults in the Mojave Desert and limited geologic slip rate estimates, it is premature to claim a geologic versus geodetic “discrepancy” for the ECSZ. More data are needed to provide a statistically meaningful assessment of the geologic rates for each of the faults comprising the ECSZ.

References

Atwater, T., and Stock, J. (1998), Pacific-North America plate tectonics of the Neogene southwestern United States: an update. International Geology Review, 40(5), 375-402.

Becker, T. W., Hardebeck, J. L., and Anderson, G. (2005), Constraints on fault slip rates of the southern California plate boundary from GPS velocity and stress inversions. Geophysical Journal International, 160(2), 634-650.

Bennett, R. A., Rodi, W., and Reilinger, R. E. (1996), Global Positioning System constraints on fault slip rates in southern California and northern Baja, Mexico. Journal of Geophysical Research: Solid Earth, 101(B10), 21943-21960.

Blewitt, G., Kreemer, C., Hammond, W. C., and Gazeaux, J. (2016), MIDAS robust trend estimator for accurate GPS station velocities without step detection. Journal of Geophysical Research: Solid Earth, 121.

Chuang, R. Y., and Johnson, K. M. (2011), Reconciling geologic and geodetic model fault slip-rate discrepancies in Southern California: Consideration of nonsteady mantle flow and lower crustal fault creep. Geology, 39(7), 627-630.

Cooke, M. L., and Dair, L. C. (2011), Simulating the recent evolution of the southern big bend of the San Andreas fault, southern California. Journal of Geophysical Research: Solid Earth, 116(B4).

Dawson, T. E., and Weldon II, R. J. (2013), Appendix B: Geologic slip-rate data and geologic deformation model. US Geol. Surv. Open-File Rept.

DeMets, C., and Dixon, T. H. (1999), New kinematic models for Pacific-North America motion from 3 Ma to present, I: Evidence for steady motion and biases in the NUVEL-1A Model. Geophysical Research Letters, 26(13), 1921-1924.

DeMets, C., Gordon, R. G., and Argus, D. F. (2010), Geologically current plate motions. Geophysical Journal International, 181(1), 1-80.

DeMets, C., and Merkouriev, S. (2016), High-resolution reconstructions of Pacific–North America plate motion: 20 Ma to present. Geophysical Journal International, 207(2), 741-773.

Dixon, T. H., Robaudo, S., Lee, J., and Reheis, M. C. (1995), Constraints on present-day Basin and Range deformation from space geodesy. Tectonics, 14(4), 755-772.

Dixon, T. H., Miller, M., Farina, F., Wang, H., and Johnson, D. (2000), Present-day motion of the Sierra Nevada block and some tectonic implications for the Basin and Range province, North American Cordillera. Tectonics, 19(1), 1-24.

Dixon, T. H., Norabuena, E., and Hotaling, L. (2003), Paleoseismology and Global Positioning System: Earthquake-cycle effects and geodetic versus geologic fault slip rates in the Eastern California shear zone. Geology, 31(1), 55-58.

Dokka, R. K., and Travis, C. J. (1990a), Late Cenozoic strike-slip faulting in the Mojave Desert, California. Tectonics, 9(2), 311-340.

Dokka, R. K. and Travis, C. J. (1990b), Role of the eastern California shear zone in accommodating Pacific-North American plate motion. Geophysical Research Letters, 17(9), 1323-1326.

Dolan, J. F., Bowman, D. D., and Sammis, C. G. (2007), Long-range and long-term fault interactions in Southern California. Geology, 35(9), 855-858.

Dolan, J. F., and Haravitch, B. D. (2014), How well do surface slip measurements track slip at depth in large strike-slip earthquakes? The importance of fault structural maturity in controlling on-fault slip versus off-fault surface deformation. Earth and Planetary Science Letters, 388, 38-47.

Evans, E. L., Thatcher, W. R., Pollitz, F. F., and Murray, J. R. (2016), Persistent slip rate discrepancies in the eastern California (USA) shear zone. Geology, 44(9), 691-694.

Frankel, K.L., Glazner, A.F., Kirby, E., Monastero, F.C., Strane, M.D., Oskin, M.E., Unruh, J.R., Walker, J.D., Anandakrishnan, S., Bartley, J.M., Coleman, D.S., Dolan, J.F., Finkel, R.C., Greene, D., Kylander-Clark, A., Marrero, S., Owen, L.A., Phillips, F., 2008. Active tectonics of the eastern California shear zone. In: Duebendorfer, E.M., Smith, E.I. (Eds.), Field guide to Plutons, Volcanoes, Faults, Reefs, Dinosaurs, and Possible Glaciation in Selected Areas of Arizona, California, and Nevada: Geol. Soc. Am. field Guide, 11, 43-81, doi: 10.1130/2008.fl d011(03).

Frankel, K.L., Owen, L.A., Dolan, J.F., Knott, J.R., Lifton, Z.M., Finkel, R.C. and Wasklewicz, T., (2015), Timing and rates of Holocene normal faulting along the Black Mountains fault zone, Death Valley, USA. Lithosphere, 8(1), 3-22.

Gan, W., Svarc, J. L., Savage, J. C., and Prescott, W. H. (2000), Strain accumulation across the Eastern California Shear Zone at latitude 36 30′ N. Journal of Geophysical Research: Solid Earth, 105(B7), 16229-16236.

Gourmelen, N., Dixon, T. H., Amelung, F., and Schmalzle, G. (2011), Acceleration and evolution of faults: An example from the Hunter Mountain–Panamint Valley fault zone, Eastern California. Earth and Planetary Science Letters, 301(1), 337-344.

Gray, H. J., Owen, L. A., Dietsch, C., Beck, R. A., Caffee, M. A., Finkel, R. C., and Mahan, S. A. (2014), Quaternary landscape development, alluvial fan chronology and erosion of the Mecca Hills at the southern end of the San Andreas fault zone. Quaternary Science Reviews, 105, 66-85.

Hedrick, K.A., Owen, L.A., Chen, J., Robinson, A., Yuan, Z., Yang, X., Imrecke, D.B., Li, W., Caffee, M.W., Schoenbohm, L.M. and Zhang, B. (2016), Quaternary history and landscape evolution of a high-altitude intermountain basin at the western end of the Himalayan-Tibetan orogen, Waqia Valley, Chinese Pamir. Geomorphology.

Herbert, J. W., Cooke, M. L., Oskin, M., and Difo, O. (2014a), How much can off-fault deformation contribute to the slip rate discrepancy within the eastern California shear zone?. Geology, 42(1), 71-75.

Herbert, J. W., Cooke, M. L., and Marshall, S. T. (2014b), Influence of fault connectivity on slip rates in southern California: Potential impact on discrepancies between geodetic derived and geologic slip rates. Journal of Geophysical Research: Solid Earth, 119(3), 2342-2361.

Hidy, A. J., Gosse, J. C., Pederson, J. L., Mattern, J. P., and Finkel, R. C. (2010), A geologically constrained Monte Carlo approach to modeling exposure ages from profiles of cosmogenic nuclides: An example from Lees Ferry, Arizona. Geochemistry, Geophysics, Geosystems, 11(9).

Hidy, A. (2013), Cosmogenic Nuclide Quantification of Paleo-fluvial Sedimentation Rates in Response to Climate Change. Ph.D Thesis, Dalhousie University, Halifax.

Liu, S., Shen, Z. K., and Bürgmann, R. (2015), Recovery of secular deformation field of Mojave shear zone in southern California from historical terrestrial and GPS measurements. Journal of Geophysical Research: Solid Earth, 120(5), 3965-3990.

Loveless, J. P., and Meade, B. J. (2011), Stress modulation on the San Andreas fault by interseismic fault system interactions. Geology, 39(11), 1035-1038.

Malservisi, R., Furlong, K. P., and Dixon, T. H. (2001), Influence of the earthquake cycle and lithospheric rheology on the dynamics of the eastern California shear zone. Geophysical Research Letters, 28(14), 2731-2734.

McCaffrey, R. (2005), Block kinematics of the Pacific–North America plate boundary in the southwestern United States from inversion of GPS, seismological, and geologic data. Journal of Geophysical Research: Solid Earth, 110(B7).

McClusky, S. C., Bjornstad, S. C., Hager, B. H., King, R. W., Meade, B. J., Miller, M. M., and Souter, B. J. (2001), Present day kinematics of the eastern California shear zone from a geodetically constrained block model. Geophysical Research Letters, 28(17), 3369-3372.

McGill, S. F., Spinler, J. C., McGill, J. D., Bennett, R. A., Floyd, M. A., Fryxell, J. E., and Funning, G. J. (2015), Kinematic modeling of fault slip rates using new geodetic velocities from a transect across the Pacific-North America plate boundary through the San Bernardino Mountains, California. Journal of Geophysical Research: Solid Earth, 120(4), 2772-2793.

McQuarrie, N., and Wernicke, B. P. (2005), An animated tectonic reconstruction of southwestern North America since 36 Ma. Geosphere, 1(3), 147-172.

Meade, B. J. and Hager, B. H. (2005), Block models of crustal motion in southern California constrained by GPS measurements. Journal of Geophysical Research: Solid Earth, 110(B3).

Miller, M. M., Johnson, D. J., Dixon, T. H., and Dokka, R. K. (2001), Refined kinematics of the Eastern California shear zone from GPS observations, 1993–1998. Journal of Geophysical Research: Solid Earth, 106(B2), 2245-2263.

Minster, J. B., and T. H. Jordan (1987), Vector constraints on western U.S. deformation from space geodesy, neotectonics, and plate motions, Journal of Geophysical Research, 92(B6), 4798–4804.

Oskin, M., and Iriondo, A. (2004), Large-magnitude transient strain accumulation on the Blackwater fault, Eastern California shear zone. Geology, 32(4), 313-316.

Oskin, M., Perg, L., Blumentritt, D., Mukhopadhyay, S., and Iriondo, A. (2007), Slip rate of the Calico fault: Implications for geologic versus geodetic rate discrepancy in the eastern California shear zone. Journal of Geophysical Research: Solid Earth, 112(B3).

Oskin, M., Perg, L., Shelef, E., Strane, M., Gurney, E., Singer, B., and Zhang, X. (2008), Elevated shear zone loading rate during an earthquake cluster in eastern California. Geology, 36(6), 507-510.

Owen, L. A., Frankel, K. L., Knott, J. R., Reynhout, S., Finkel, R. C., Dolan, J. F., and Lee, J. (2011), Beryllium-10 terrestrial cosmogenic nuclide surface exposure dating of Quaternary landforms in Death Valley. Geomorphology, 125(4), 541-557.

Peltzer, G., Crampé, F., Hensley, S., and Rosen, P. (2001). Transient strain accumulation and fault interaction in the Eastern California shear zone. Geology, 29(11), 975-978.

Rockwell, T. K., Lindvall, S., Herzberg, M., Murbach, D., Dawson, T., and Berger, G. (2000), Paleoseismology of the Johnson Valley, Kickapoo, and Homestead Valley faults: Clustering of earthquakes in the eastern California shear zone. Bulletin of the Seismological Society of America, 90(5), 1200-1236.

Sauber, J., Thatcher, W., Solomon, S. C., and Lisowski, M. (1994), Geodetic slip rate for the eastern California shear zone and the recurrence time of Mojave Desert earthquakes. Nature, 367(6460), 264-266.

Selander, J. A. (2015), Mechanisms of Strain Transfer Along Strike-Slip Faults: Examples From the Mojave Desert, California. Ph.D Thesis, University of California, Davis.

Shelef, E., and Oskin, M. (2010), Deformation processes adjacent to active faults: Examples from eastern California. Journal of Geophysical Research: Solid Earth, 115(B5).

Shen, Z. K., King, R. W., Agnew, D. C., Wang, M., Herring, T. A., Dong, D., and Fang, P. (2011), A unified analysis of crustal motion in Southern California, 1970–2004: The SCEC crustal motion map. Journal of Geophysical Research: Solid Earth, 116(B11).

Spinler, J. C., Bennett, R. A., Anderson, M. L., McGill, S. F., Hreinsdóttir, S., and McCallister, A. (2010), Present-day strain accumulation and slip rates associated with southern San Andreas and eastern California shear zone faults. Journal of Geophysical Research: Solid Earth, 115(B11).

U.S. Geological Survey and California Geological Survey (2006), Quaternary fault and fold database for the United States, accessed 16 June 2016, from USGS web site: http//earthquakes.usgs.gov/hazards/qfaults/.

Ward, S. N. (1990), Pacific-North America Plate motions: New results from very long baseline interferometry. Journal of Geophysical Research: Solid Earth, 95(B13), 21965-21981.

Zechar, J. D., and Frankel, K. L. (2009), Incorporating and reporting uncertainties in fault slip rates. Journal of Geophysical Research: Solid Earth, 114(B12).

Figures

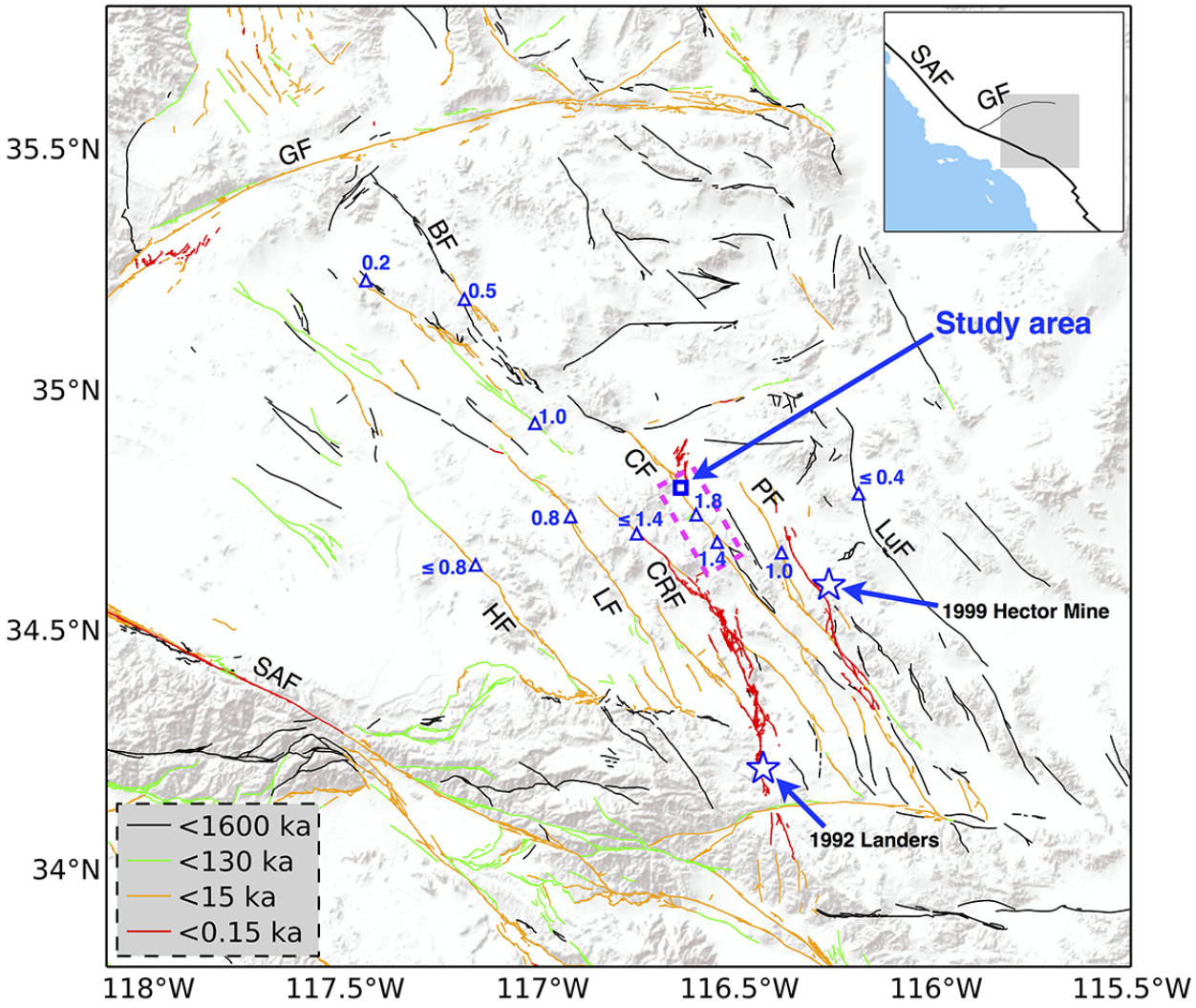

Figure 1. Fault map of area shows the ECSZ in the Mojave Desert region. Faults downloaded from the U.S. Geological Survey and California Geological Survey [2006], color indicates the time of recent movement. Blue triangles show locations of geologic strike-slip rate estimates from recent studies, with rates given in mm/yr [Oskin and Iriondo, 2004; Oskin et al., 2007, 2008; Selander, 2015]. Blue stars show locations of the 1992 M_w 7.3 Landers earthquake and the 1999 M_w 7.1 Hector Mine earthquake. Blue cubic box shows location of the geologic site in this study. Dashed magenta box outlines the area of Figure 11. SAF – San Andres fault; GF – Garlock fault; HF – Helendale fault; LF – Lenwood fault; CRF – Camp Rock fault; CF – Calico fault; BF – Blackwater fault; PF – Pisgah fault; LuF – Ludlow fault.

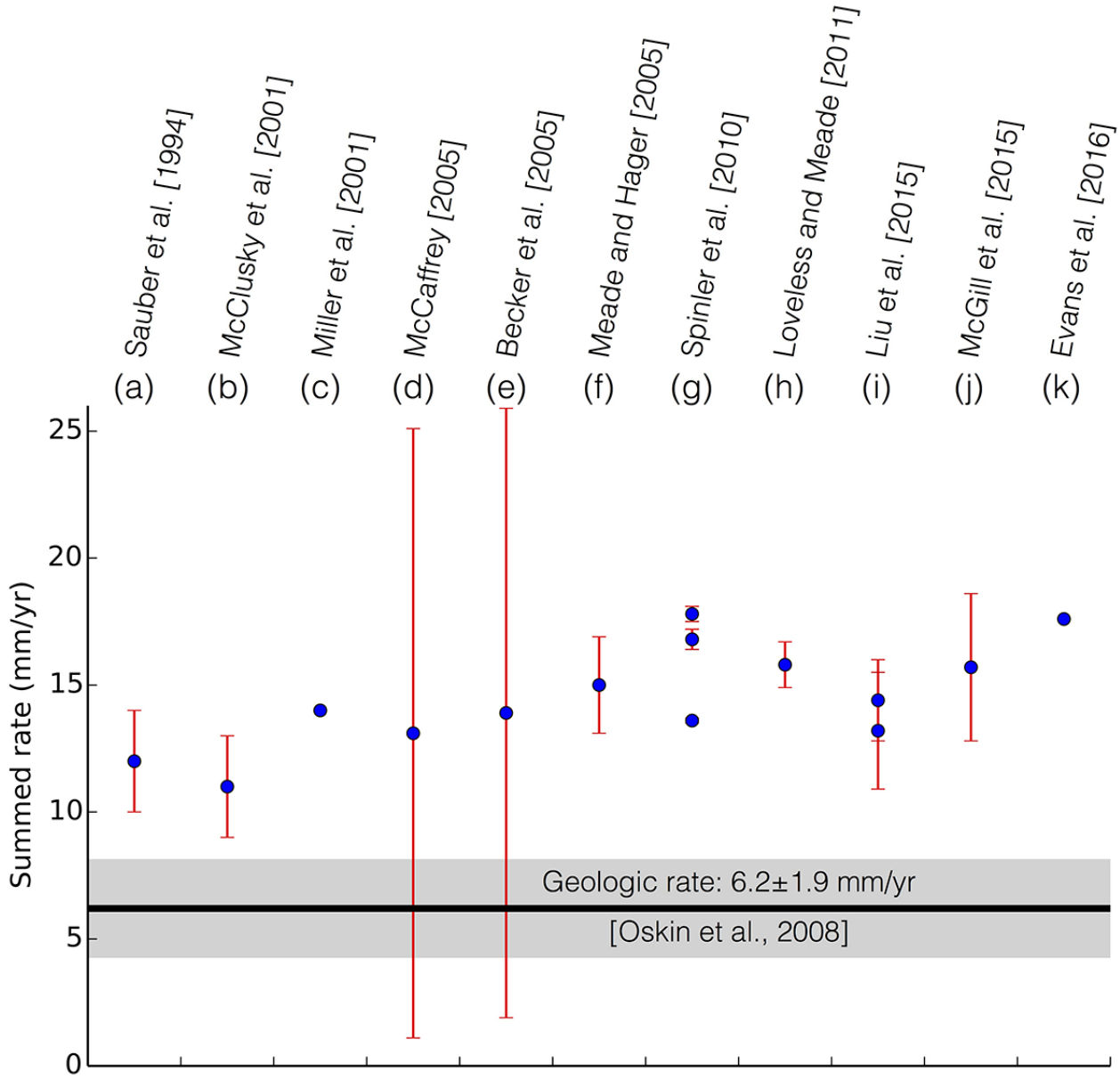

Figure 2. Summed geodetic and geologic rates. Black line and gray area mark the summed geologic slip rate and its uncertainty (2σ, 95% confidence interval) from Oskin et al. [2008]. Blue dots with error bars represent summed geodetic rates and their uncertainties (1σ, 68% confidence interval) from elastic deformation models (a) – (k). Note that slip rates of (d) [McCaffrey, 2005] and (h) [Loveless and Meade, 2011] are calculated at latitude 34.8° N based on their block models.

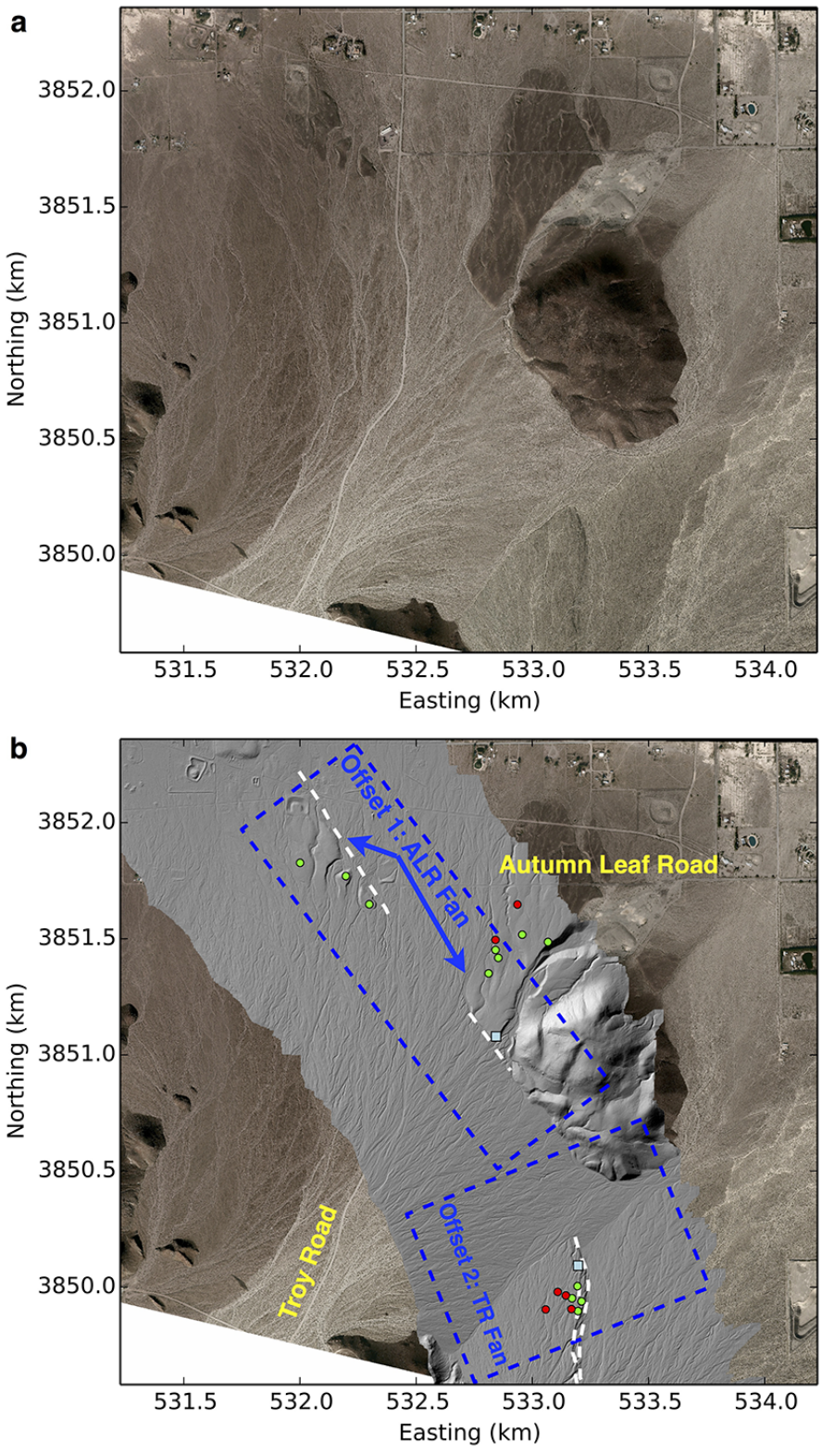

Figure 3. Image of the study area. (a) Aerial image. (b) LiDAR hillshade overlain on aerial image. Blue dashed boxes outline two offset landforms shown in Figure 4 and 5. White dashed lines indicate mapped fault traces. Red and lime green dots show locations of rock samples (red dots represent samples used in age estimates). Two sky-blue cubes are locations of two trenches: CalicoA on the ALR alluvial fan and Calico-Pit2 on the TR alluvial fan. The coordinates are in UTM zone 11 N.

Figure 4. Displacement of ALR alluvial fan (offset 1 outlined in Figure 3). (a) Displacements measure from various wash margins matched from both sides of the Calico fault. Yellow dots mark the prominent drainages on the fan surfaces. (b) Restoration of 1120 m of right-lateral slip on the Calico fault. Use width of the major channel as 2σ error (95% confidence interval). (c) Hillshade of the restoration by using LiDAR derived DEM.

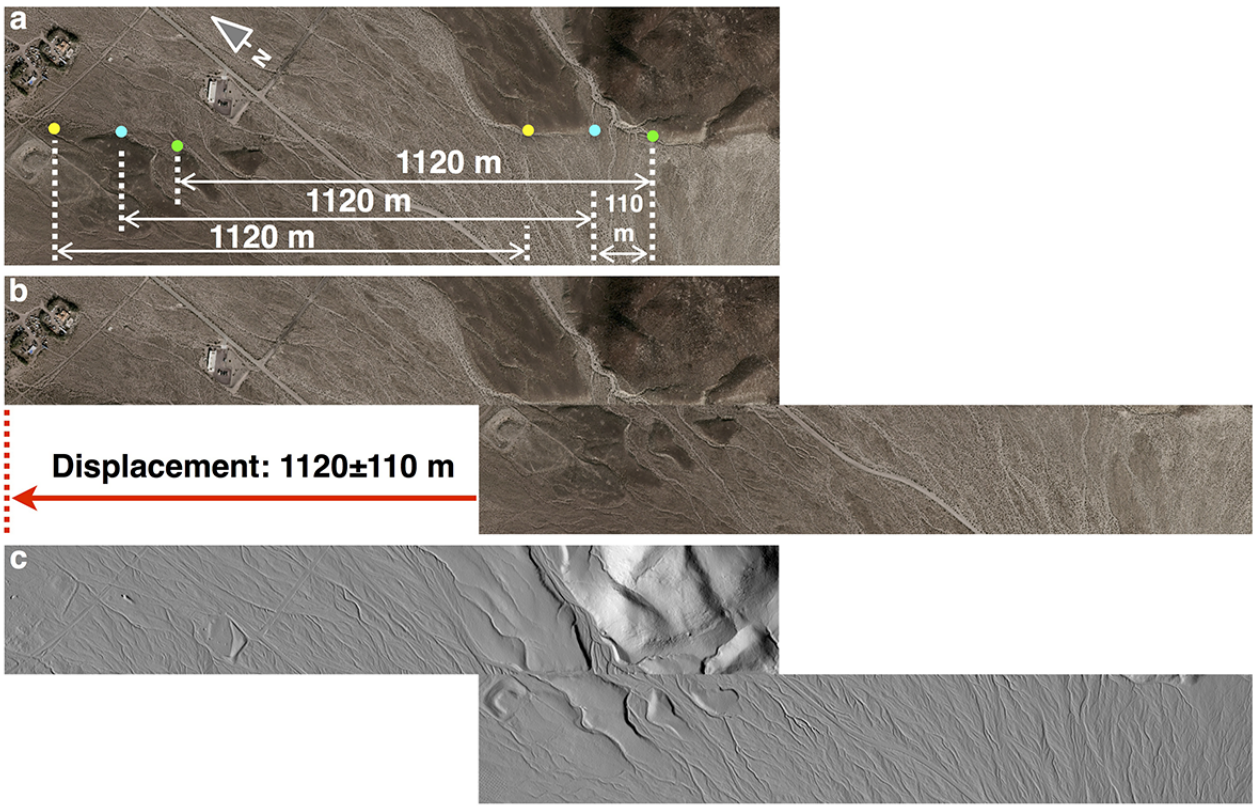

Figure 5. Displacement of TR alluvial fan (offset 2 outlined in Figure 3). (a1-a3) Restorations of displacement on aerial image. (b1-b3) Restorations of displacement on LiDAR derived DEM. (c1-c3) Restorations of displacement on slope aspect derived from LiDAR DEM. The minimum displacement estimate is 90 m when aligning the linear downstream channel with the oldest upstream fan edge (a2, b2, c2); the maximum estimate of 205 when taking the inter-median surface as part of the TR alluvial fan (a3, b3, c3).

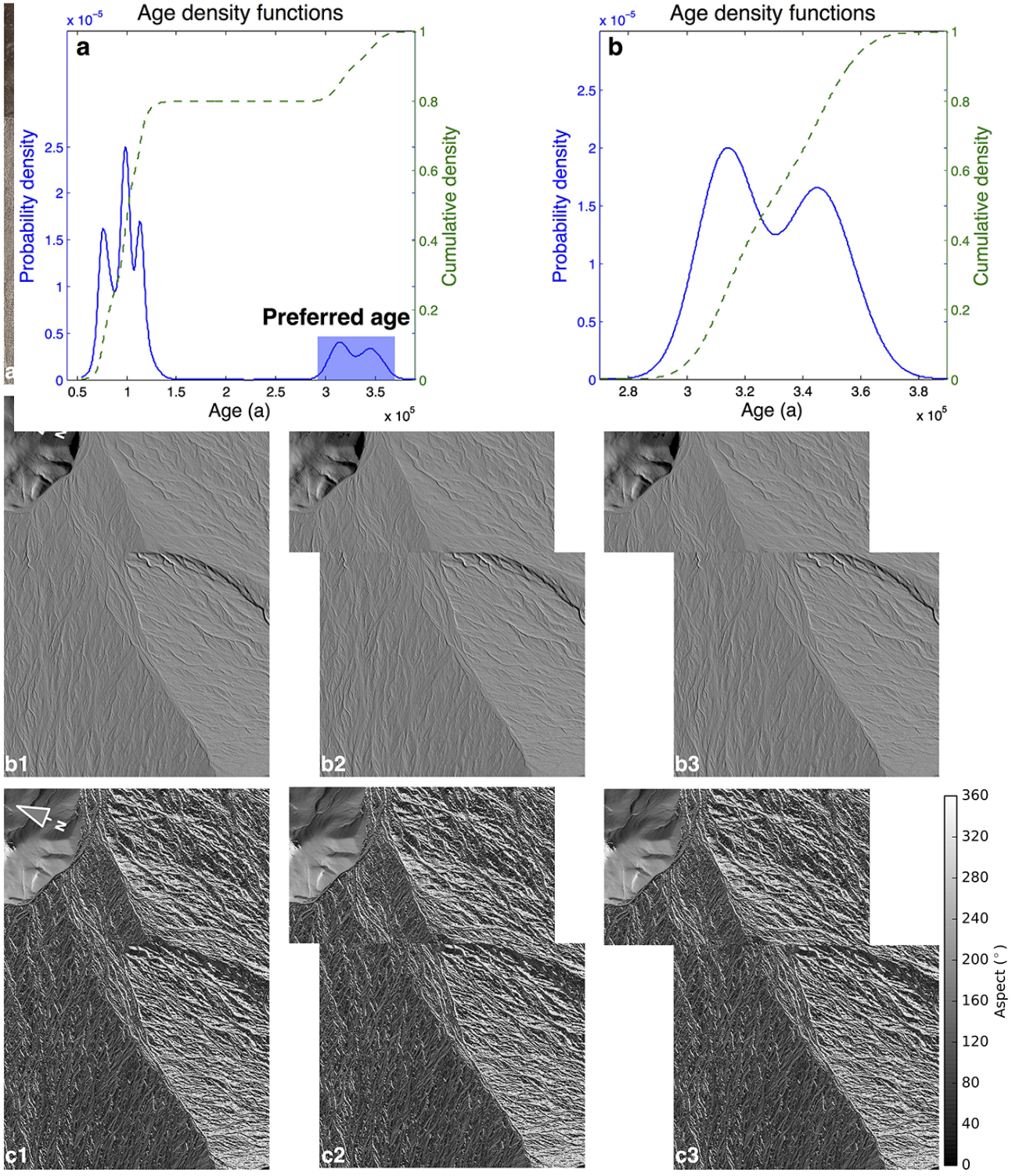

Figure 6. Age probability density function (PDF) of rock sample on ALR alluvial fan. (a) Age PDF for all rock samples. Based on soil development and age PDF of the depth profile (Figure 7), ages ~100 ka are considered as outliers. (b) PDF after outliers removed, age estimate is 328.4 $^{+37.9}/_{-32.0}$ ka (95% confidence interval). We simplify the age as normal distribution with 2σ error space of ±37.9 ka.

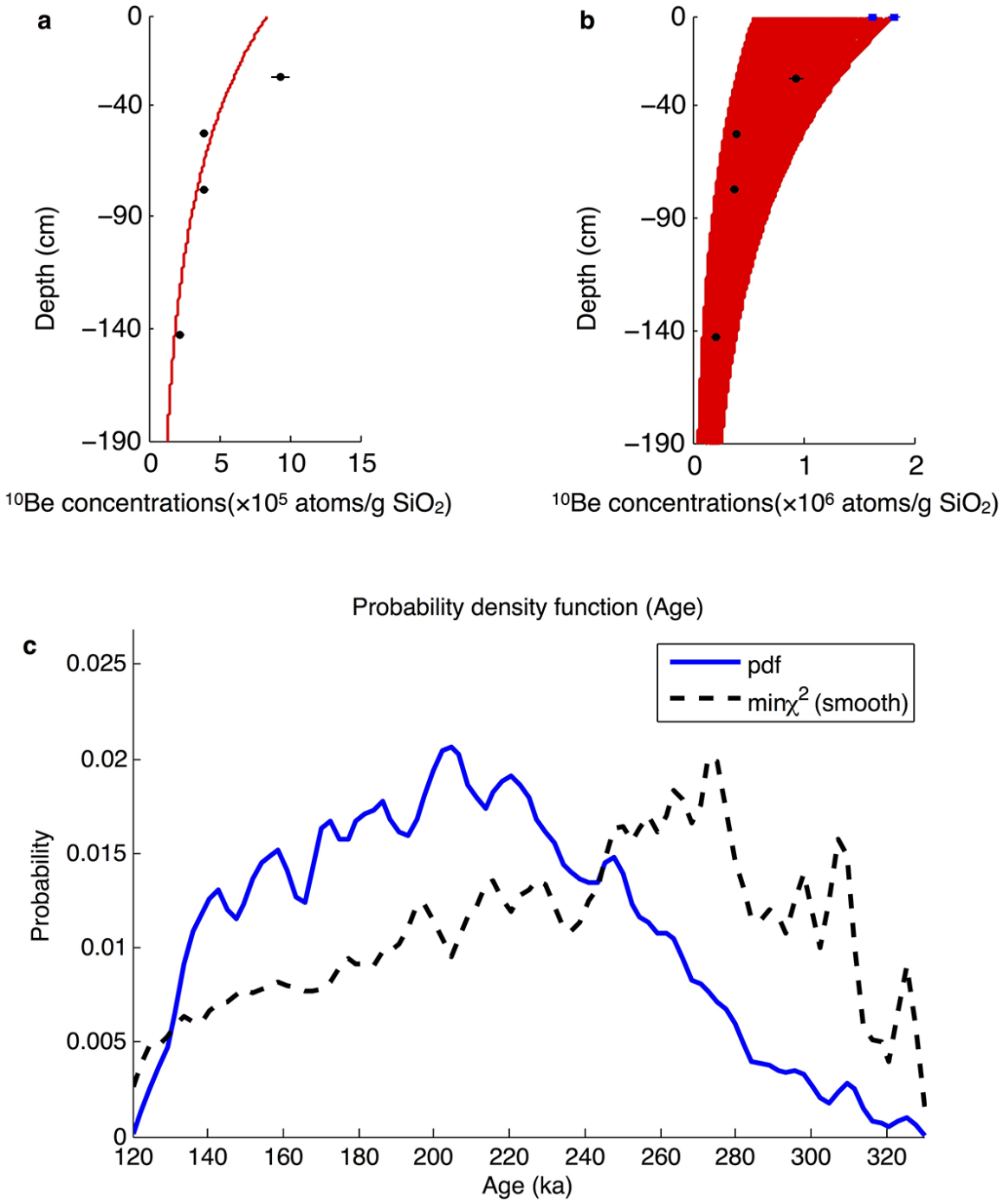

Figure 7. Surface exposure age estimate for the depth profile of CaliCoA on ALR alluvial fan. (a) Sample depth versus ^{10}Be concentration, red curve is the best fit from 100,000 Bayesian-Monte Carlo simulations using the methods of Hidy et al. [2010] and Hidy [2013]. Black dots with error bar (2□) show ^{10}Be concentration of samples. (b) 95% confidence interval solution space (red) for the 100,000 Bayesian-Monte Carlo profile simulations. Blue squares with error bar (2σ) show ^{10}Be concentration of two rock samples on the fan surface. The inheritance estimate (4×10^4 atoms/g) is very low and we don't show it in the figure. (c) Age PDF from 100,000 Bayesian-Monte Carlo simulations. The Bayesian most probable age is 204.5 $^{+91.7}/_{-71.9}$ ka (95% confidence interval). We simplify the age as normal distribution with 2σ error space of ±91.7 ka.

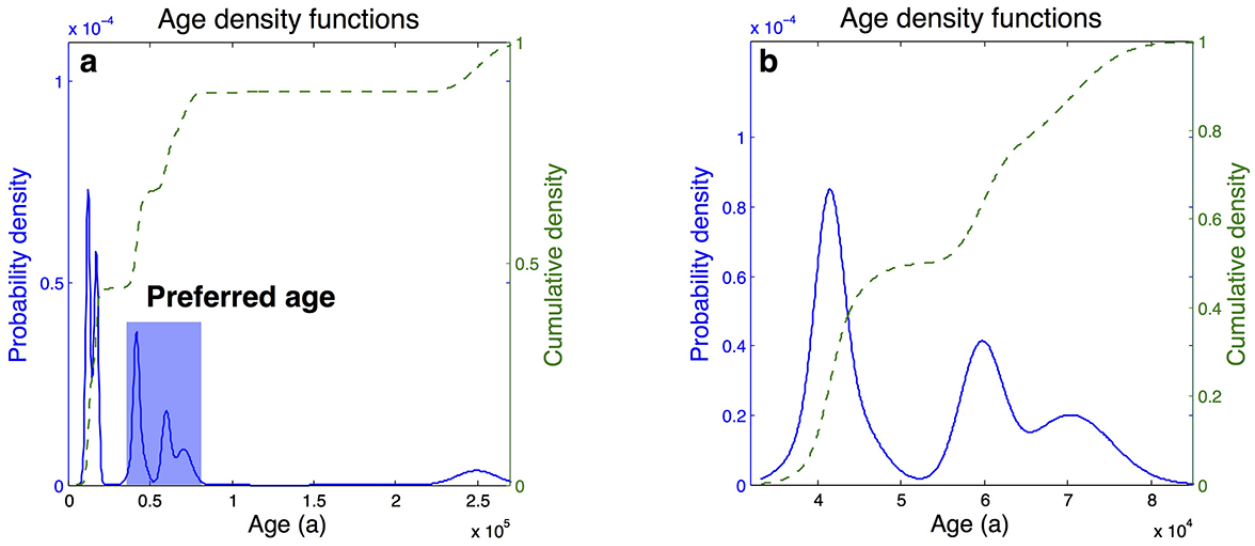

Figure 8. Age probability density function (PDF) of rock sample on TR alluvial fan. (a) Age PDF for all rock samples. Samples with age ~15 ka are taken as outliers, and these are all near the secondary fault tract. The sample with an age of ~250 ka is most likely to have large inheritance from other much older units, so we consider it as an outlier. (b) PDF after outliers removed, age estimate is 52.9 $^{+23.6}/_{-15.7}$ ka (95% confidence interval). We simplify the age as normal distribution with 2σ error space of ±23.6 ka.

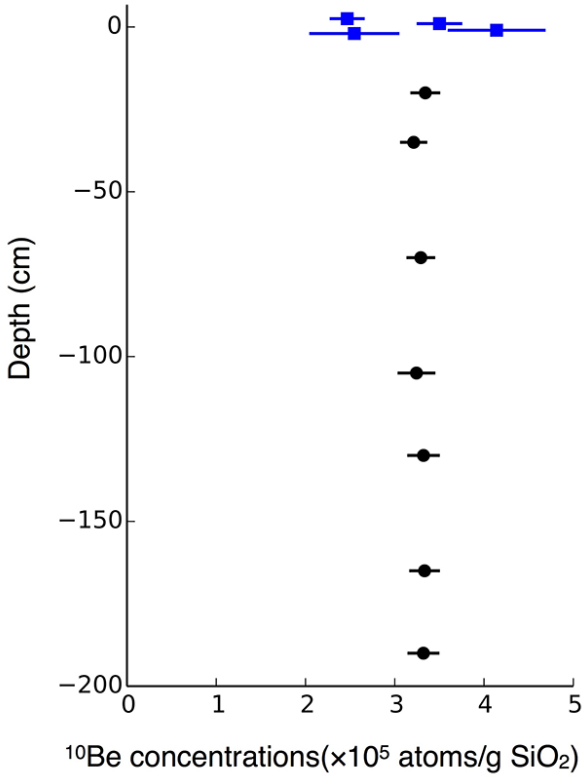

Figure 9. Sample depth versus ^{10}Be concentration for the Calico-Pit2 trench from the TR alluvial fan. Black dots with error bar (2σ) show ^{10}Be concentration of depth samples. Blue squares with error bar (2σ) show ^{10}Be concentration of four rock samples on the alluvial fan surface (dislocate slightly on vertical direction to avoid overlapping).

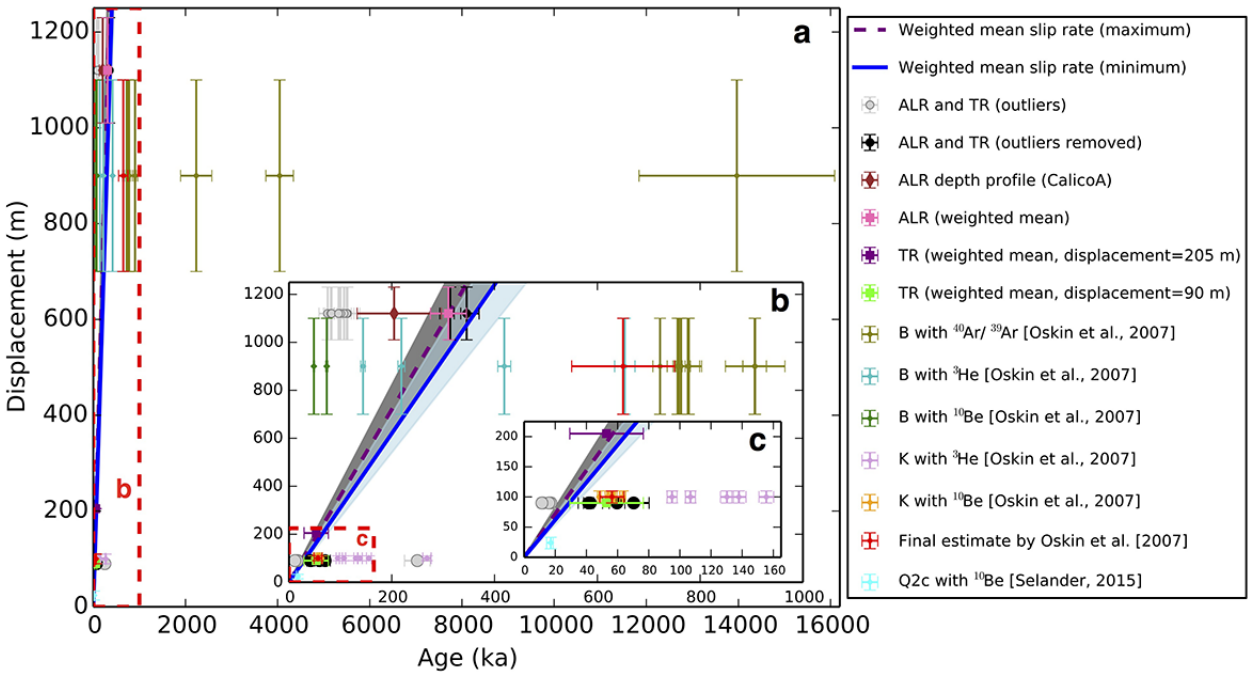

Figure 10. Age, displacement and slip rate estimates for the Calico fault. Dashed red boxes outline inserted figure b and c. For clarity, ages of rock samples from TR alluvial fan are only plotted with minimum displacement. All error bars represent two standard deviations. Blue line and light blue area shows weighted mean slip rate and its 2σ error for the Calico fault when using the minimum displacement estimate for the TR alluvial fan; dashed purple line and grey area show slip rate and 2σ error when using the maximum displacement estimate for the TR alluvial fan.

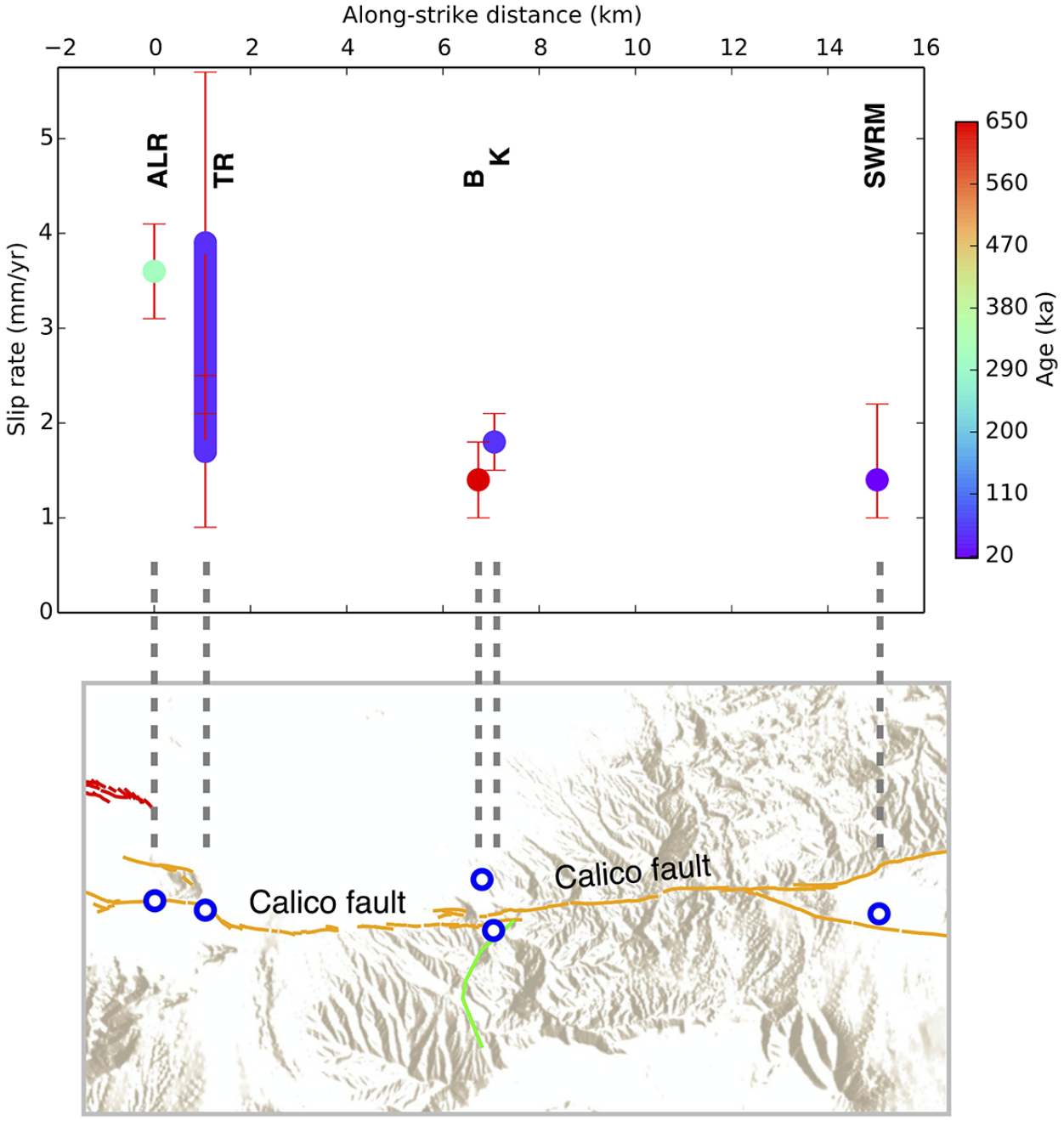

Figure 11. Along-strike slip rate estimates on the Calico fault. Fault map shows the area outlined by dashed magenta box in Figure 1. Color represents age. ALR: 3.6±0.5 mm/yr from this study; TR: 1.7±0.8 to 3.9±1.7 mm/yr from this study; B: 1.4±0.4 mm/yr from Oskin et al. [2007]; K: 1.8±0.3 mm/yr from Oskin et al. [2007]; SWRM: $1.4\ ^{+0.8}/_{-0.4}$ mm/yr from Selander [2015] (southwest Rodman Mountains).

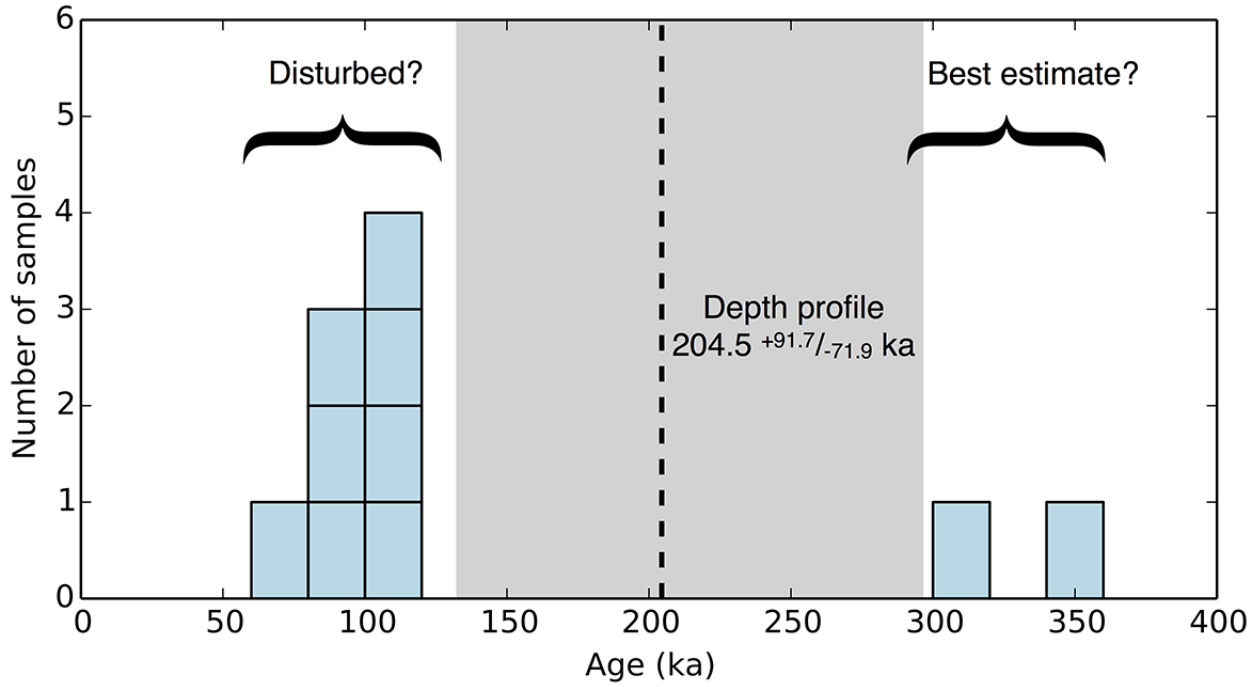

Figure 12. Sample age distribution of the ALR alluvial fan. Each box indicates a rock sample, dashed line and grey area show the age and uncertainty estimates of the depth profile CalicoA.

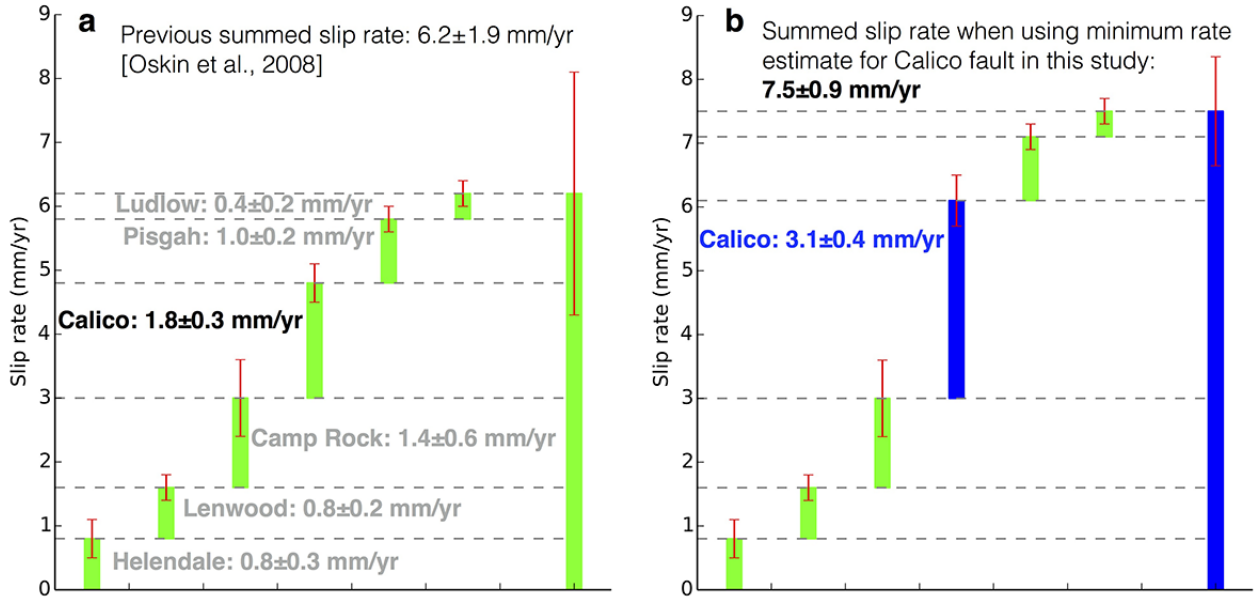

Figure 13. Summed geologic slip rate for major faults across the Mojave ECSZ. (a) Previous published results. (b) Summed slip rate when using minimum displacement estimate for the TR Fan in this study. Error space (95% confidence interval) in this study is by adding all errors in quadrature (root of summed squares).

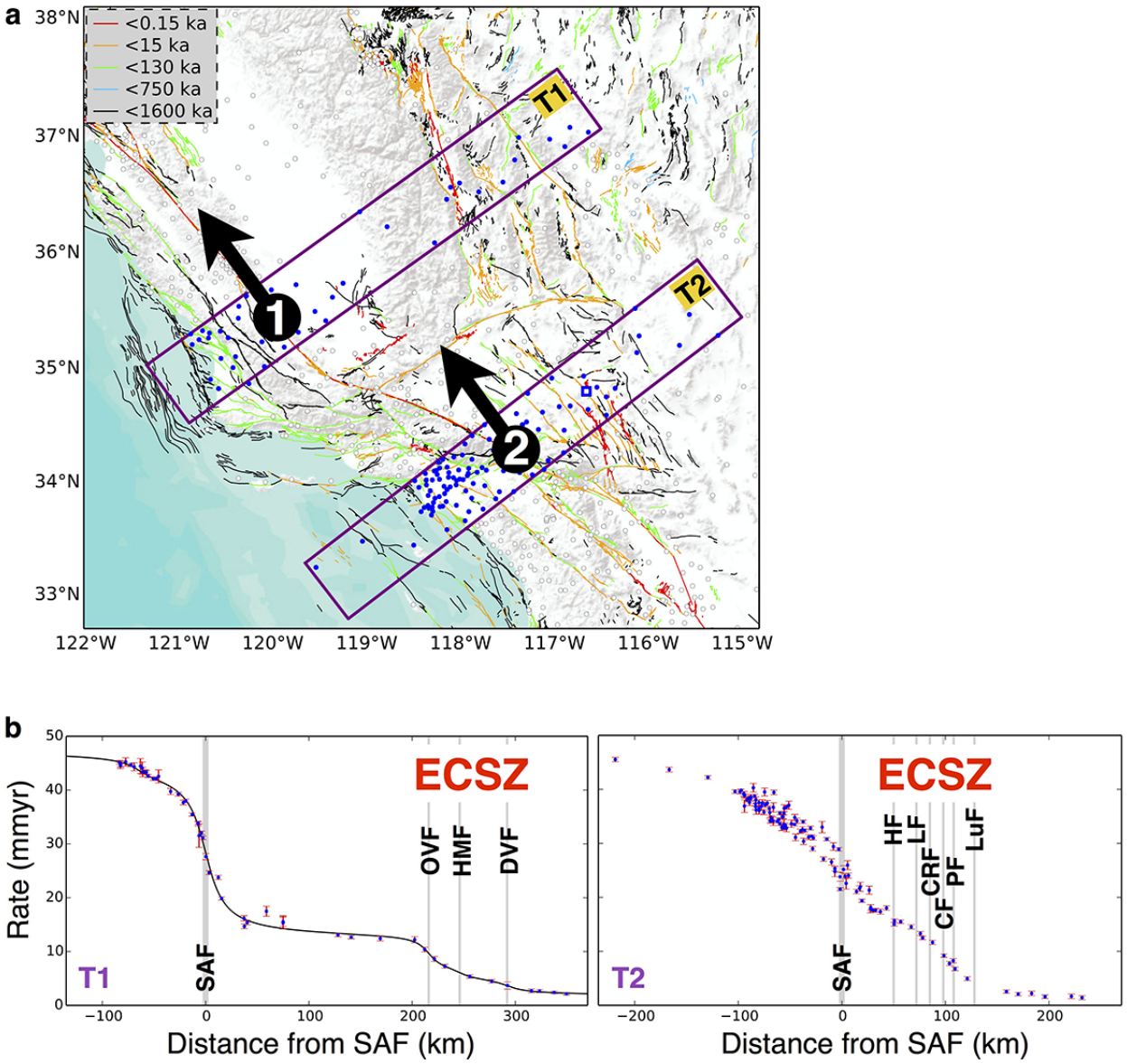

Figure 14. Geodetic slip rate across the ECSZ. (a) Two transects (T1, T2, 485 km × 70 km) across the ECSZ. Blue dots are GPS stations within these two transects, white dots are GPS stations out of the transects. Point 1 (35.45° N, 120.0° W) on SAF moves 48.4 mm/yr, point 2 (34.29° N,117.5° W) moves 47.4 mm/yr (Pacific plate to North America plate). Blue box shows location of the study area in this study. Plate motion model from DeMets and Merkouriev [2016]. (b) GPS velocities of transects T1 and T2. Velocities are in plate boundary parallel direction. Grey lines show locations of the major faults across the ECSZ. For T1, summed geodetic slip rate from the three major ECSZ faults of Owens Valley fault (OVF), Hunter Mountain fault (HMF) and Death Valley fault (DVF) is 11.2±0.6 mm/yr (2σ, keep consistent with geologic estimates). GPS velocities are from Blewitt et al. [2016].